SPE 122133

New Insights into Application of Foam for Acid Diversion

Rouhollah Farajzadeh[1,2], Alexey Andrianov[1], Hans Bruining[2], Pacelli L.J. Zitha[1,2]

[1] SPE, Shell International Exploration and Production, Rijswijk, The Netherlands
[2] SPE, Department of Geotechnology, Delft University of Technology, The Netherlands

This paper was prepared for presentation at the 2009 SPE European Formation Damage Conference held in Scheveningen, The Netherlands, 27–29 May 2009.

Abstract

Foam is widely used to divert acid or abandon the high permeable layers. In this type of application foam should considerably reduce gas mobility. The nature of the gas and the surfactant may influence foaming behavior and thus the efficiency of the foam. In this paper an experimental study of the behaviorof CO_2 and N_2 foams in granular porous media using X-ray Computed Tomography is reported. In the experiments gas is forced through natural porous media initially saturated with a surfactant solution, a process known as SurfactantAlternatingGas (SAG). The CO_2 was either under sub- or super-critical conditions whereas N_2 remained under subcritical conditions in all experiments. Alpha Olefin Sulfonate (AOS) surfactant was used as foaming agent. We found that injection of gas following a slug of surfactant can considerably reduce gas mobility and promote higher liquid recovery at the experimental conditions investigated. Foaming of CO_2 builds-up a lower pressure drop over the core at both low and high pressures than N_2. Both gases require a certain penetration depth to develop into foam. This length is longer for N_2 (larger entrance effect) and increases with growing gas velocity. Moreover, the ultimate liquid recovery by CO_2 foam is always lower than by N_2 foam. The possible mechanisms explaining the observed differences in foaming behavior of the two gases are discussed in detail.

1. INTRODUCTION

Foam in porous media is a gas-liquid mixture with a continuous liquid phase wetting the rock whereas a part or all of the gas is made discontinuous by thin liquid films called lamellae [1-3]. Foam has been widely used to block the high-permeability layers and divert the injected fluid, for instance acid, to the damaged/unswept layers [4-7]. In these applications foam reduces the gas mobility by trapping a large part of the gas. Moreover, the foam reduces the liquid mobility by reducing the gas mobility in flowing fraction of foam [8]. Foams have been also used to improve the oil recovery of some fields [9-11]. The success of a foam application relies on the properties of rock and the foam itself. These include parameters such as surfactant concentration, surfactant adsorption on rock, foam propagation in porous media (foam strength/stability) and reservoir heterogeneity (and wettability). The physico-chemical properties of the injected gas can also play an important role in efficiency of foam in porous media.

The growing concern about the global warming and shortage of energy supply has increased the interest in combined geological CO_2 storage and Enhanced Oil Recovery applications [12-14]. Although the geological storage of CO_2 is considered as an attractive solution for global warming, the efficiency (or even feasibility) of the process is not yet established [15]. One major problem is the leakage of the injected CO_2 through the walls of abandoned wells or through the cap rock [16]. In this case the foaming of CO_2 may temporarily hamper the leakage while other actions are considered.

There are two main injection strategies in Enhanced Oil Recovery (EOR) field projects related to foam. These are the co-injection of gas and liquid, and surfactant alternating gas (SAG) injection. In the first strategy the gas and liquid are co-injected at a fixed ratio. The ratio between the gas flowrate and the sum of the gas and liquid flowrates (thus, total flowrate) determines the foam quality. The foam can also be generated outside the porous medium before the injection; however, we categorize this strategy under the co-injection scheme. In the SAG scheme alternating slugs of surfactant solution and gas are injected and, therefore, foam is generated inside the porous medium (in-situ generation) [1,17,18]. The SAG foam is sometimes called *drainage foam* in the literature [19]. In the recent EOR application of foam in the Snorre field offshore Norway the SAG phase operations were conducted without any major problem while the co-injection was hampered by

operational problems that resulted in unstable injectivity [20,21]. In fact, the SAG process is similar to water alternating gas process (WAG) and requires a little additional effort [5,17-22]. SAG injection minimizes contact between water and gas in surface facilities and piping, which can be important when the gas, e.g. CO_2, forms an acid upon contact with water [23,24]. The laboratory study of Huh and Handy [25] also revealed that the gas-surfactant co-injection foam can completely block the porous medium under certain conditions, while this never occurs with the SAG foam. It was also shown that the mobility reduction factor is higher for co-injection foam than for SAG foam at the same gas flowrate.

While the co-injection foam has been the center of attention of many experiments [26-31], there is only a little data on the SAG foam [18,32-34]. Moreover, in most of the previous studies on foam flow in porous media the measured pressure drop became stationary only after 10-100 pore volumes of the injected fluids (liquid and gas). In these experiments the pressure drop does not increase significantly until the gas phase reaches the end of the initially surfactant saturated porous medium, a phenomenon that cannot be explained by the existing models [35]. Possibly, this happens due to high gas flowrates or short length of the core often used in experiments. Indeed, the injected gas needs to travel inside the porous medium before it mixes with the available surfactant and foams. However, when the gas flowrate is high or the porous medium is short, the gas will breakthrough before development of a strong foam. The gas will only start to form a strong foam in the laboratory set-up if many pore volumes are injected. Therefore, the obtained results can only be representative of the initial stage of the injection process. It has been also observed that various gases behave differently, both in bulk [36-38] and porous media [18,39-42] experiments. Recently, Du et al. [27] showed experimentally that there is essential difference between CO_2 and N_2 foams in porous media. In their experiments the gases were co-injected with Sodium Dodecyl Sulfate (SDS) solution at high injection rates. The differences were attributed to the dissimilar physical properties of the gases, mainly higher CO_2 solubility in water compared to N_2.

Our objective is to study the effect of the gas type on the behavior of foam in porous media, at both low and high pressure and temperatures. In the experiments, CO_2 or N_2 gas is injected into the core that is initially saturated with a surfactant solution (SAG foam). Section 2 describes the experimental set-up, materials and procedure. Section 3 presents the results for two sets of experiments. The first set of experiments is performed at atmospheric pressure and room temperature of $T=20^oC$. The second set of experiments is conducted at $P=90$ *bar* and $T=50^oC$. This condition is well above the critical point of CO_2. Section 4 provides detailed explanation of the differences observed in the experiments and investigates the relevant physical/chemical properties of gases affecting the foam behavior in the porous medium. Finally, we draw the main conclusions of this study.

2. EXPERIMENTAL

2.1 CT imaging

The values of the CT scanner are measured in Hounsfield units (HU). The relationship between attenuation coefficient and HU is:

$$HU_m = 1000\left(\frac{\mu_m}{\mu_w} - 1\right) \tag{1}$$

where μ_w displays the water attenuation coefficient: we obtain $HU_m = 0$ for water and $HU_m = -1000$ for air. The following equation is used to compute the liquid saturation, S_w, from the measured HU, eliminating the contribution of the rock by the subtraction:

$$S_w = \frac{HU_{foam} - HU_{dry}}{HU_{wet} - HU_{dry}} \tag{2}$$

where the subscripts foam, wet and dry stand for the foam flow, solution saturated and dry core conditions, respectively.

2.2. Materials

Chemicals: The surfactant used was alpha-olefin sulfonate, AOS (Stepan company, The USA). This surfactant is anionic and was used as received without any further purification. The general structure of olefin surfactants is $R\text{-}SO_3^-Na^+$, where *R* represents the hydrophobic group. In our case the number of the carbon atoms in the surfactant structure is *12* and the molecular weight of the surfactant is $M_w=273$ *g/mol*. A fixed active surfactant concentration of $c_{AOS}=0.50$ *wt%* was used in our experiments. Sodium chloride (NaCl) was used to make the Brine. The concentration of NaCl was a fixed value of 0.5M (*~3 wt%*) in all experiments reported here. All solutions were prepared with deionized water ($pH=6.8\pm0.1$). In order to increase the CT attenuation of the solutions, *10 wt%* of Sodium Wolframate (Aldrich, 99% purity) was added to the solutions.

Gases: The gases used to carry out the experiments were *99.98%* pure CO_2 and N_2. The solubility of CO_2 in water is about *55* times higher than that of nitrogen [46].

Porous Media: The porous medium used was consolidated, quasi-homogenous and quartz-rich Bentheimer sandstone. The main properties of the porous medium are presented in Table 1. The permeability was calculated from the pressure data of a single-phase (brine) flow (with a known flowrate) through the core and the porosity was determined from the CT data. The radius of the pore throats are mainly in the range of *10-30 μm.*

2.3. Experimental Set-up

The schematic of the experimental set-up is schematically shown in Fig. 1. It consists of four parts: Injection Unit (IU), Test Unit (TU), Pressure Controlling Unit (PCU) and Data Acquisition System (DAS).

Injection Unit: In order to ensure the supply of the gas at a stable rate, the gas flow rate is controlled by using a high precision needle valve (for low-pressure experiments) and an ISCO pump (for high pressure experiments) and it is monitored by using a gas flow meter. A high precision double-effect piston displacement pump (Pharmacia P 500) is used to inject the brine and the surfactant solution at a constant rate.

Test Unit: In the test unit, the sample core is placed inside a cylindrical coreholder. The coreholder is made of PolyEthylene EtherKetone (PEEK) that combines good mechanical properties to a low X-ray attenuation. The geometry and structure of the core holder were designed to minimize beam hardening and scattering artifacts [47]. The core holders were placed vertically on the platform of the CT scanner apparatus and kept in place using a polymethyl methacrylate (PMMA) stand. The foam is introduced from the injection tube, and the liquid production is collected in a glass cup on an electronic mass balance. Two high precision pressure transducers locate at the inlet and the outlet to monitor the pressure drop along the core.

Pressure Control Unit: The pressure control part connects to the outlet of the core. By using a backpressure regulator and a manometer we can measure different pressures in the system. The data acquisition system records gas and liquid injection rates, pressures and the liquid production data automatically. All experiments are conducted under isothermal conditions. The low pressure experiments are done at room temperature of T=20 ^{o}C and the high pressure experiments are performed at a constant temperature of T=50 ^{o}C.

Most of the core-flood set-up is positioned on the table of the CT scanner. The PEEK core holder is vertically placed, perpendicular to the length of the table, to control the gravity segregation effects. The third generation SAMATOM Volume Zoom Quad slice scanner is used in our work. The main technical information about this machine has been provided elsewhere [26] and the imaging settings in our experiments are listed in Table 2. The X-ray tube of the CT scanner is operated at the voltage of *140 kV* and the current of *250 mA*. The thickness of CT slice is *3 mm* and one series of scan includes *4* slices. In the calculations the slice corresponding to the center of the core was used.

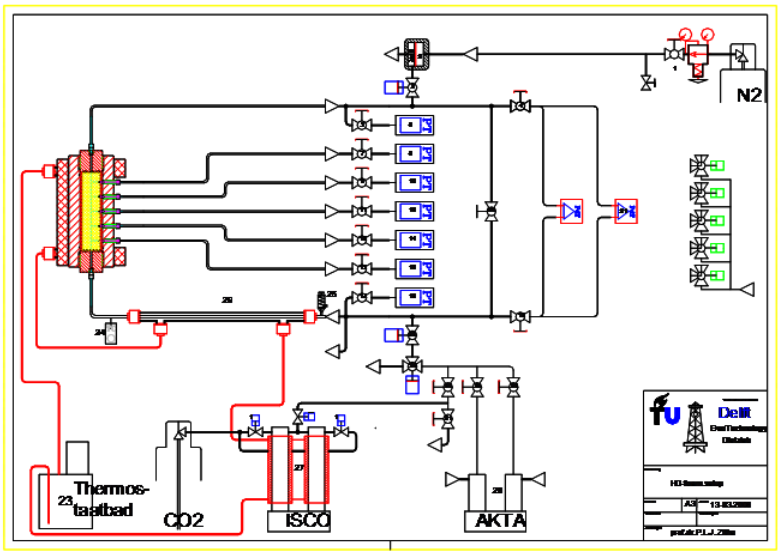

Figure 1: Schematic of the foam set-up: It consists of four major units: injection unit (pumps), test unit (the porous medium), pressure controlling unit and data acquisition system (not shown in this Fig.).

Table 1: Properties of sandstone cores (porous media)

Name	Permeability [mD]	Porosity [%]	Diameter [mm]	Length [mm]	Pore Volume [ml]	Main composition
Long core	1010	22±0.2	40±1	170±2	42.5±0.5	Quartz
Short core	1010	22±0.2	40±1	90±2	22.5±0.5	Quartz

Table 2: Settings of the CT scan measurements

PARAMETERS	CT-scan settings
Energy Levels [keV]	140
Current [mA]	250
Slice Thickness [mm]	3
Number of Slices	4
Filter	B40-medium

2.4. Experimental Procedure

Core Preparation: The cores were drilled from a large block and sawn to the dimensions specified in Table 1 using a diamond saw cooled with water. The cores were dried in an oven at *60°C* for at least *48* hours. Then the cores were molded in Araldite glue to avoid production from the axial core sides. The core was then placed in a PEEK core holder. For pressure measurements inside the core, the pressure gauges were connected through a small hole drilled in the glue to the surface of the core. The connectors were also made of PEEK to reduce the beam-hardening effects of X-ray beam.

Before starting the experiments all of the connections in the set-up were checked for possible leakages by keeping the set-up under high pressure and monitoring the measured pressures.

Core Saturation: The core was flushed with CO_2 for at least *30* minutes to replace the air in the system. Afterwards, at least *20* pore volumes of brine with the flowrate of q_w*=2 ml/min* were injected to the system while the backpressure was set P_b*=20 bar*. Therefore, all CO_2 present in the core is dissolved into the brine and carried away. This is confirmed by CT images.

Surfactant Injection: After the core was saturated with the brine, 1 pore volume of the surfactant was injected (q_s*=2 ml/min*) to the porous medium. The adsorption of AOS surfactant on Bentheimer sandstone is very low [45]. Moreover, *1wt%* of AOS is well above its CMC value [44] and therefore, injection of 1 PV of surfactant would be sufficient to satisfy the rock adsorption.

Foam (gas) Injection: The gas is injected into the core previously saturated with the surfactant solution (SAG foam).

3. RESULTS

3.1. Low pressure foam development

a) CT scan images: Figure 2 presents the CT images of the central part of the CO_2 and N_2 experiments respectively. The time of each image is also shown in terms of the dimensionless time of pore volumes, *PV*, which is the ratio of the cumulative volume of injected fluids (in these experiments only gas) to the volume of the pore space in the porous medium. In these experiments the gas (CO_2 or N_2) was injected with a flowrate of *0.5 ml/min* to the core initially saturated with *1-2 PV* of the surfactant solution (SAG scheme). The blue and red colors represent the gas and the liquid phases, respectively. The general features of these experiments (foam advance) are similar to foam experiments in which the surfactant solution and the gas are co-injected into the porous medium [27]. For both CO_2 and N_2, the images show a front-like displacement of the aqueous phase by foam. Three regions can be distinguished in both experiments along the flow direction: 1) an upstream region which is characterized by low liquid saturation, 2) a region downstream of the foam front where the liquid saturation is still unchanged and equals unity and 3) a frontal region characterized by a mixing of flowing foam and liquid and exhibits fine fingering effects. The extent of the fingering behavior is caused by the local rock heterogeneity [26,28] and apparently depends on the type of the foamed gas (foam strength).

Nevertheless, a closer examination of the images reveals the considerable differences between CO_2 and N_2 foams. About *0.30 PV* of CO_2 is injected before the gas penetrates the core and becomes visible in the images while N_2 becomes visible much more rapidly as the gas penetrates the core immediately displacing the liquid. This is possibly due to the higher solubility of CO_2 in water. The upstream region of CO_2 foam front is less blue indicating higher water content compared to the upstream region of N_2 foam. However, similar to N_2 foam, as the foam front progresses in the core, the gas sweeps parts of the remaining liquid from the upstream region towards the outlet. In the frontal region, N_2 foam is sharper than CO_2. Finally the

higher solubility of CO_2 in the aqueous phase results in its substantially delayed breakthrough. The gas breakthrough takes places at a time between *1.30* and *1.70 PV* for N_2 foam while the foamed CO_2 breaks through at a time slightly larger than *2.20 PV*.

The amount of CO_2 that can be dissolved in water can be estimated by Henry's law. The solubility of CO_2 in water is ~*34 mol/m*^{3} at our experimental condition. Using the CT images the volume of water that gas has met was estimated at each *PV* and then the amount of dissolvable CO_2 was calculated. The results are summarized in Table 3. In these calculations the possible effect of surfactant micelles on CO_2 solubility is disregarded. It turns out that the amount of dissolved CO_2 is considerable and therefore the effect of water solubility cannot be neglected [27]. Indeed, considering also some dead volume in the system, more than *1 PV* of the injected CO_2 is required to saturate the liquid before it can form foam.

b) Saturation profiles: To quantify the evolution of the liquid saturations, S_w, over the entire core, the CT data of the obtained images were converted to water saturation profiles using Eq. (2). The results are shown in Figs. 3a and 3b at various times for CO_2 and N_2 respectively. Note that every point on these figures is the averaged water saturation over a disk of the core with ~*8 mm* thickness. These figures show that foamed CO_2 and N_2 displace the liquid, i.e., the surfactant solution from the porous medium. Prior to the gas breakthrough the saturation profiles along the core show a steep increase of S_w at the foam front, which indicates an effective front-like displacement of the initial liquid for both foams. In the case of CO_2 foam due to more fingering in the foam front, revealed by the CT images, the front is not as sharp as for the N_2 foam.

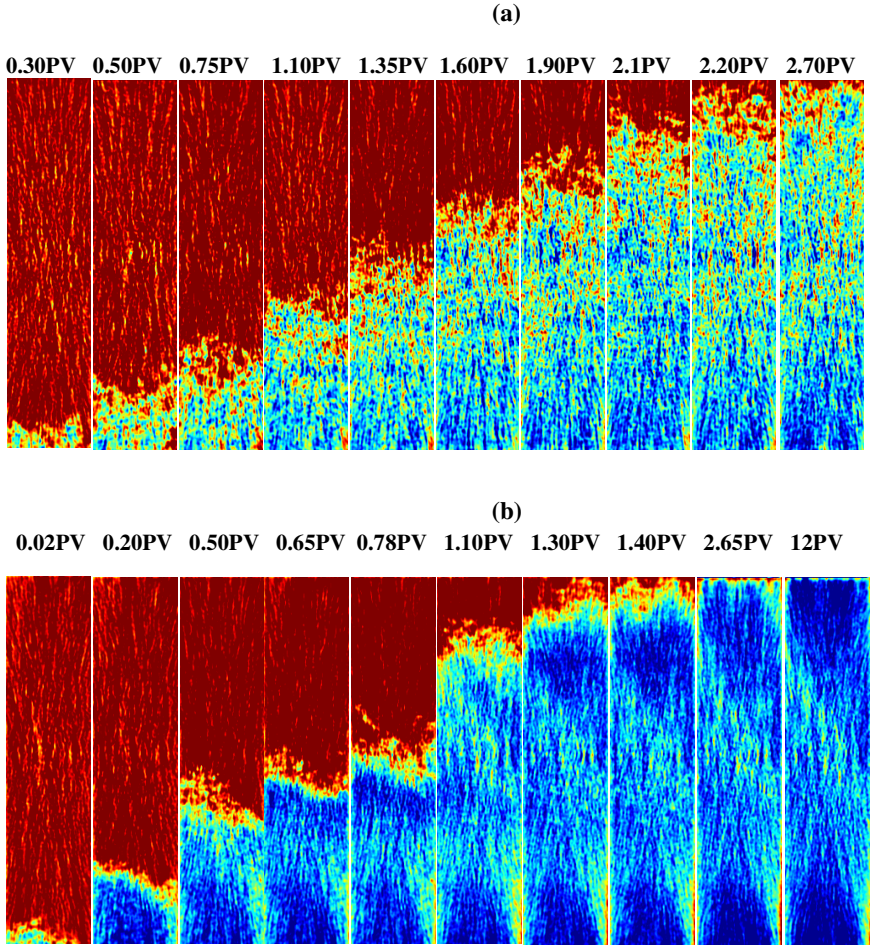

Figure 2: CT images of (a) CO_2 and (b) N_2 foam flow (blue) in a porous medium initially saturated with surfactant solution (red) at *P=1bar* and *T=20°C* (q_g*=0.5 ml/min*). The time of each image is shown in pore volumes of the injected gas.

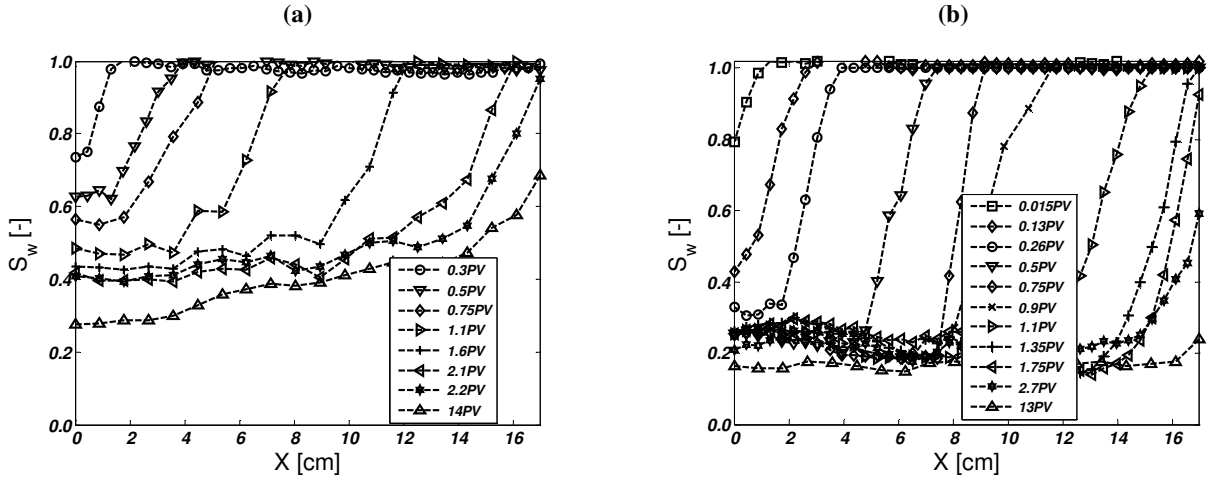

Figure 3: The liquid saturation profiles of (a) CO_2 foam and (b) N_2 foam, calculated from CT profiles shown in Fig. 2.

The high values of liquid saturation at the region close to the core outlet indicates the capillary end effect where the porous medium retains the liquid in an attempt to maintain equilibrium across the outlet where the capillary pressure is zero or near zero [49-51]. After about *2 PV* of gas injection, CO_2 foam removes about *50%* of the liquid while N_2 removes more than *70%* of the liquid. Further injection of N_2 after (foam) breakthrough removes the liquid retained at the inlet and outlet of the porous medium while further injection of CO_2 produces the liquid from the whole core as the liquid content is still high after foam breakthrough. Finally, comparing the water saturation profiles of two gases at the same pore volumes, one can conclude that the foamed N_2 displaces more liquid than foamed CO_2. Indeed, the foamed N_2 produces more than *82%* of the initial liquid in the porous medium while the foamed CO_2 sweeps less than *65%* of the initial liquid after more than *11 PV* of gas injection.

c) Pressure profiles: Figure 4 compares the measured pressure drops versus dimensionless time (PV) of the two experiments. It appears that the foamed N_2 builds up larger pressures over the core than foamed CO_2. The high liquid saturation and the small pressure drop indicate that CO_2 is in the form of relatively weak foam. Although this foam is relatively weak, it does produce a pressure drop higher than expected for the steady state pressure drop with the gas injection to a core initially saturated with water [52]. In both experiments the pressure drop across the core reaches a maximum and then decline slowly. The maximum point corresponds to the foam breakthrough at the outlet. The pressure decreases after breakthrough because of the coalescence of the bubbles due to diffusion or breaking of the foam films.

Table 3: Amount of CO_2 that can be dissolved in water calculated from Henry's law at *P=1 bar* and *T=20 °C*. The solubility of CO_2 in water at this P-T is estimated to be *34 mol/m³*.

PV of CO_2 Injected [-]	Water Content [cm^3]	Amount of dissolved CO_2 (Henry's law) [cm^3]	PV of CO_2 dissolved [-]
0.30	2.6	1.2	0.06
0.50	7.5	3.4	0.16
0.75	10.4	4.8	0.23
1.10	15.6	7.2	0.34
1.35	21.6	9.6	0.47
1.60	26.8	12.4	0.59
1.90	30.5	14.1	0.67
2.10	36.5	16.8	0.80
2.20	40.2	15	0.92
Breakthrough	42.5	19.6	0.93

For a detailed explanation of foam progress in the core the pressure drop measurements at different sections of the core are plotted for the N_2 experiments in Fig. 5. At early times, until *0.50 PV*, the pressure drop is quite small. This means that foam is still weak. From time *0.50 PV* to *0.70 PV* there is a sharp increase in the pressure drop across the beginning of the core. This is confirmed by the saturation profile in Fig. 3b. After *0.50 PV* of gas injection, the foam front moves relatively slower along the core, nevertheless, it produces more water from the upstream region. Comparing the saturation profiles of two gases, this effect is more pronounced in the CO_2 foam, possibly due to the fact that (i) CO_2 foam is weaker and (ii) unlike N_2 foam, the transition from weak to strong foam does not happen for CO_2. The low pressure drop and relatively high liquid saturation at the core inlet at early experimental times is referred to as the *entrance effect* in the literature [29,35]. Apparently gas needs

time and space before it develops into foam. The pressure drop continues to increase as gas moves forward along the core. Again due to the capillary end effect the pressure drop at the last section of the core is low (water saturation is high). The pressure drop reaches maximum of *0.42 bar* which is equal to the overall pressure drop across the core. This means that foam in the last section is weaker than foam in the first half of the core. However, as it is seen from Fig. 5 the pressure drop at the last section of the core increases with time indicating that foam becomes stronger with increasing amounts of injected gas. After foam breakthrough the pressure drop decreases due to the destruction of foam films as mentioned previously.

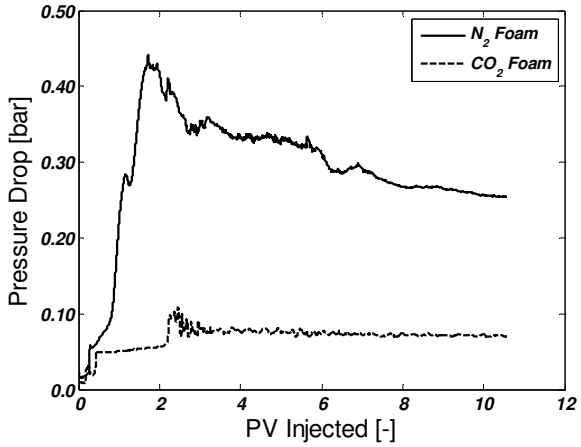

Figure 4: Pressure drop across the entire core for N_2 and CO_2 foam (q_g=0.5ml/min) at P=1bar and T=20°C

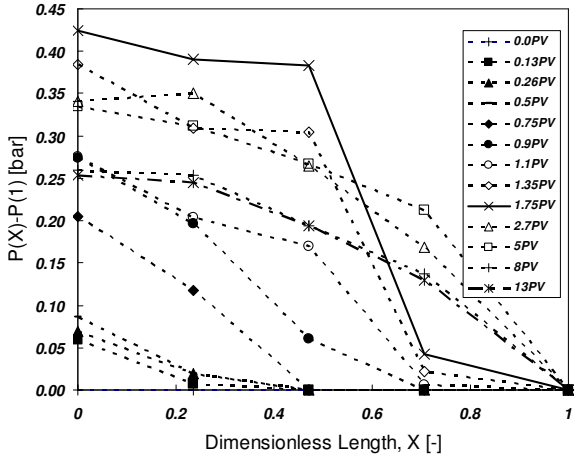

Figure 5: The transient pressure profile at different location in the core for N_2 foam experiment at *P=1bar* and *T=20°C.*

3.2. High pressure experiments

The second set of experiments were done at *P=90 bar* and *T=50°C*. This P-T condition is well above the critical point of CO_2 [53]. The density of CO_2 is 286 *kg/m*^{3} at this condition calculated from the Span and Wagner EoS [54]. Moreover, at this pressure and temperature a water-rich liquid phase coexists with a CO_2-rich liquid, where a distinction between the vapor and liquid phases of CO_2 disappears [55]. Note that foams formed with dense CO_2 as the internal phase are strictly emulsions [10], sometimes referred to as *foamulsion* [5]. However, for the sake of consistency we use the term foam here as well.

a) CT images: Figure 6 presents the central CT images of CO_2 gas, CO_2 foam and N_2 foam flow at *P=90 bar* and *T=50°C*. The time of each image is also shown in the dimensionless time of pore volumes, *PV*. The gas flowrate in these experiments was set to *1 ml/min*. In the CO_2 gas experiment the core was initially saturated with brine and CO_2 was injected into the core afterwards. The images reveal the remarkable effect of the surfactant solution in the porous medium. When CO_2 is injected to the core initially saturated with the brine, there is no (clear) sharp interface between the gas and the brine. CO_2 forms channels through the brine and breaks through in less than *0.20 PV*. When CO_2 is injected into the core initially saturated with the surfactant solution a clear interface between the moving gas and the liquid appears and CO_2 breakthrough is delayed until a time between *0.45 PV* and *0.50 PV*. The breakthrough time for N_2 foam is longer than *1.2 PV*. Similar to the low pressure foam experiments the three regions are again present at high pressure foam experiments. In the CO_2 foam, the gas bypasses part of the porous medium and therefore the brine content is high at regions near the core inlet and outlet. In the N_2 foam, the foam front moves a lot slower after *0.40 PV* which is an indication that the foam has become stronger.

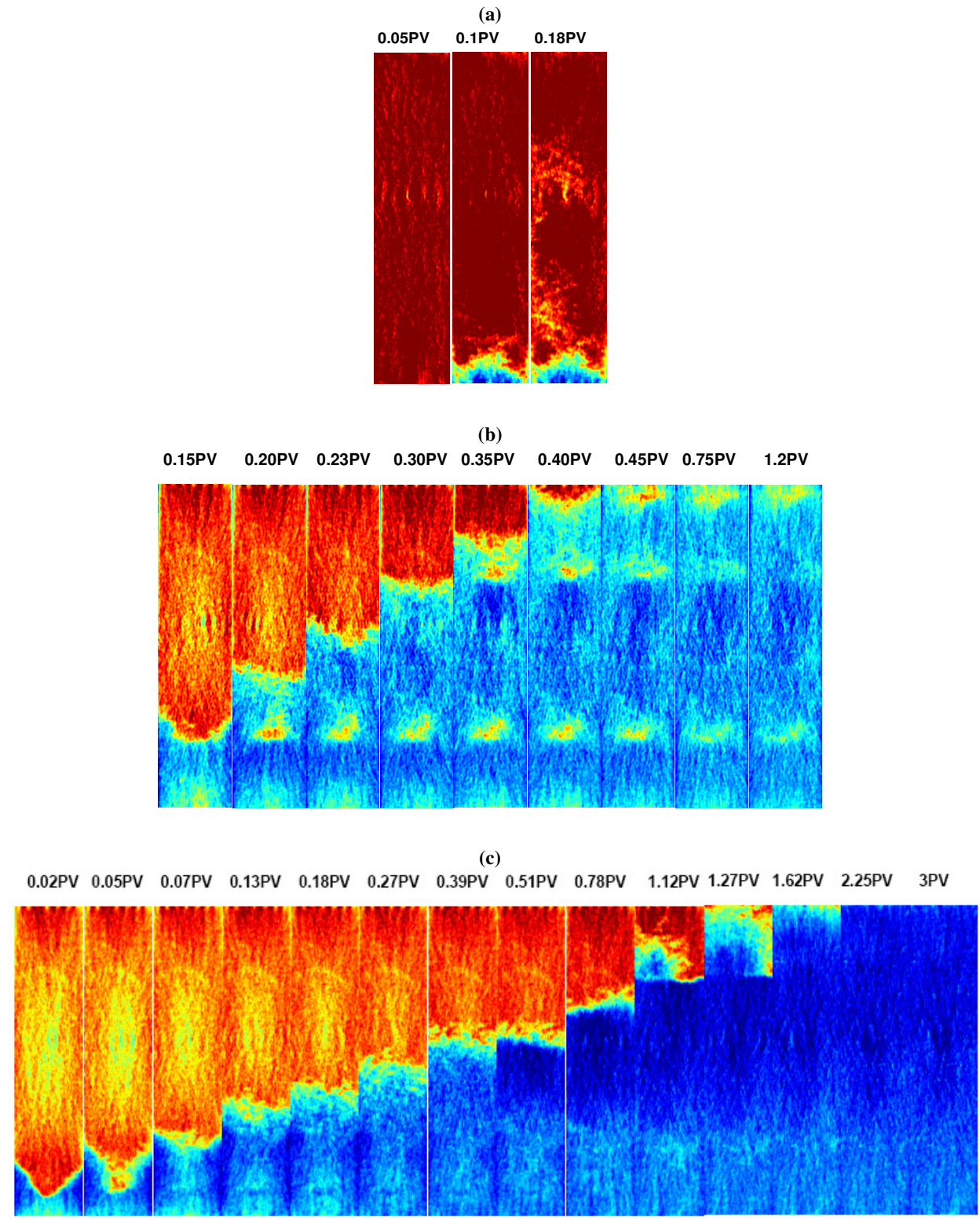

Figure 6: CT images of (a) CO_2 gas, (b) CO_2 foam and (c) N_2 foam flow in a porous medium initially saturated with surfactant solution (red) at *P=90 bar* and *T=50 °C* (q_g*=1 ml/min*). The time of each image is shown in pore volumes of the injected gas.

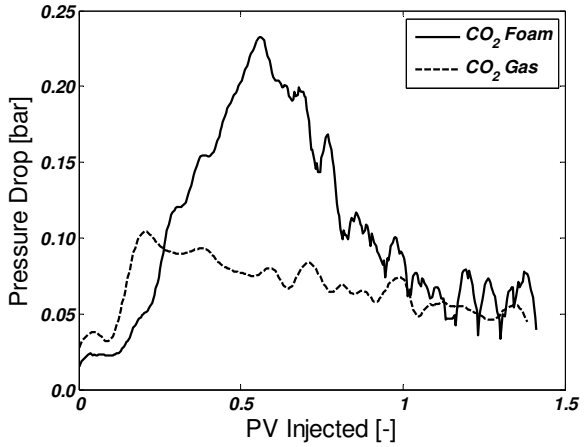

Figure 7: Pressure drop across the entire core for CO_2 gas and CO_2 foam (q_g=1 ml/min) at P=90bar and T=50°C.

b) Pressure profiles: Figure 7 shows the pressure history for CO_2 gas and CO_2 foam experiments while Fig. 8 compares the pressure drop of CO_2 and N_2 foams. The pressure drop along the core follows a similar trend; it reaches a maximum at gas breakthrough and then declines with time. The maximum value of the pressure in CO_2 foam is about two times larger than that of CO_2 gas. Compared to the low pressure experiment, the pressure peak is higher at the high pressure CO_2 (and N_2) foam because (i) the gas flowrate is higher and (ii) CO_2 has a higher density (and viscosity) in the latter case. One interesting feature is that after *1.0 PV* of CO_2 injection, the pressure drop of the CO_2 foam experiment is comparable to that of CO_2 gas experiment, meaning that after breakthrough there is almost no foam (or emulsion) present in the porous medium due to the shortage of the surfactant. The pressure drop for the N_2 foam is again larger than the CO_2 foam (see Fig. 8). In the N_2 foam the pressure drop over the core is low until *0.40 PV*, confirming the idea that gas should invade some part of the core before it develops into foam. This effect appears to be less significant for CO_2 than N_2 and as can be seen from Figs. 2 and 6, the higher the gas flowrate the larger the entrance effect is.

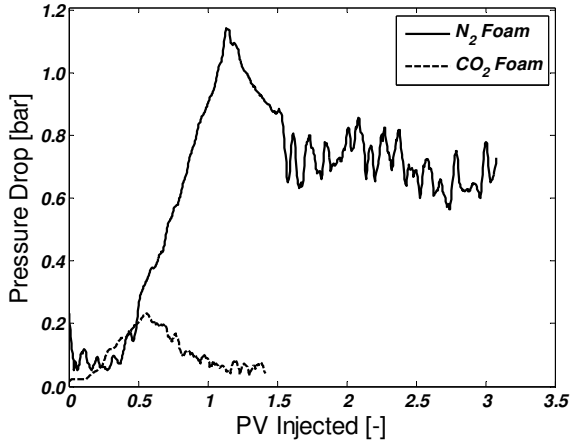

Figure 8: Pressure drop across the entire core for N_2 foam and CO_2 foam (q_g=1 ml/min) at P=90bar and T=50°C.

c) Saturation profiles: The calculated liquid saturation profiles, S_w, for the three experiments are shown in Fig. 9. In all three experiments gas displaces the liquid, although when gas is foamed inside the porous medium the amount of the liquid that remains inside the core is less than when the gas is not foamed. Moreover, in the gas injection there is no steep increase of S_w at the gas front while in foam experiments an effective front-like displacement of the initial liquid by foam takes place. The capillary end effect is present in the experiments as the liquid saturations are high near the core outlet. A detailed analysis of the N_2 foam experiments reveals that when the foam becomes stronger (after *0.40 PV* of gas injection), the liquid saturation is reduced to a value as low as *8%*; nonetheless due to the capillary end effects the saturation starts to increase to maintain the pressure equilibrium near the core outlet (This would have happened later if the core was longer). The SLD is present in this experiment because of the significance of the capillary end effects. After about *1.5 PV* of gas injection, CO_2 gas produces about *40%* of the initial liquid. Foaming of CO_2 increases the recovery by *25%* and brings out more than *65%* of the liquid. The N_2 foam removes more than *80%* of the liquid.

(a)

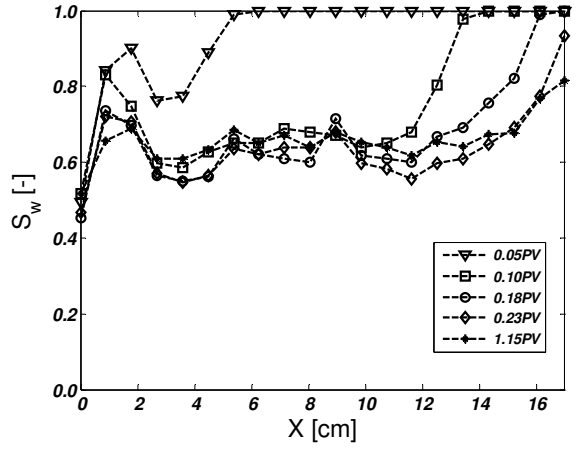

(b)

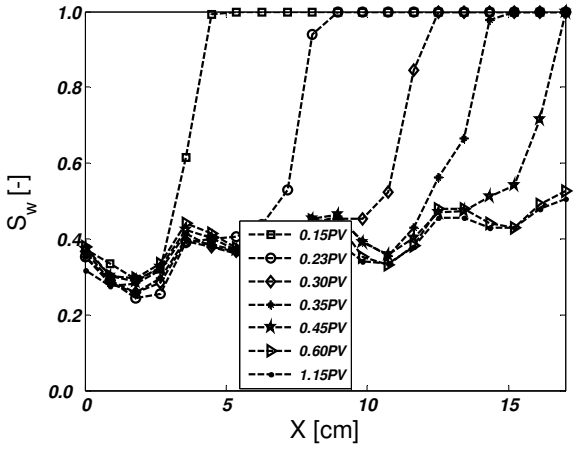

(c)

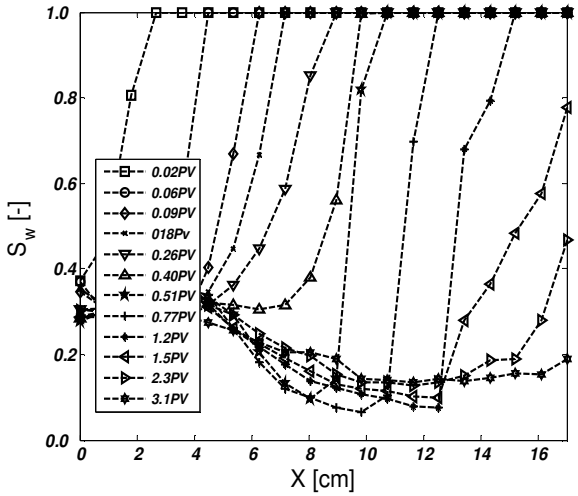

Figure 9: The liquid saturation profiles of (a) CO_2 gas (b) CO_2 foam and (b) N_2 foam, calculated from CT profiles shown in Fig. 6.

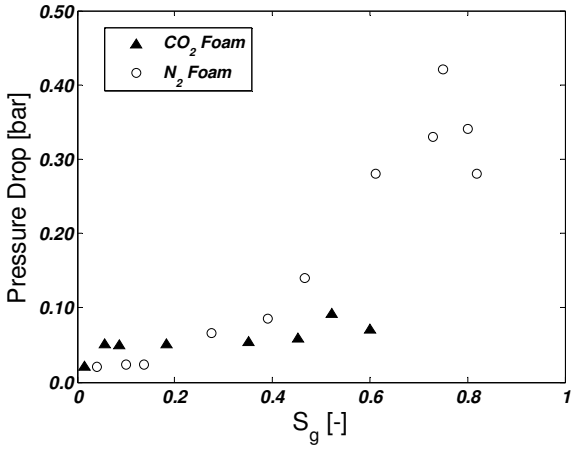

Figure 10: Pressure drop over the core vs. average gas saturation in the core for low pressure experiments [*P=1bar* and *T=20°C*].

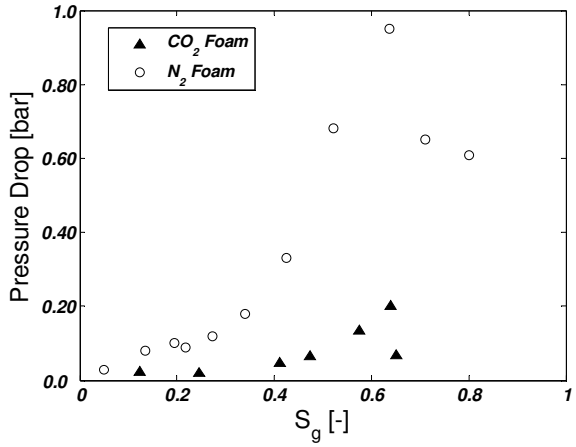

Figure 11: Pressure drop over the core vs. average gas saturation in the core for high pressure experiments [P=90bar and T=50°C].

4. GENERAL DISCUSSION

The experiments in previous sections have clearly demonstrated that under a SAG scheme CO_2 foams are *weaker* than N_2 foams at both low and high pressures. Foam in porous media is considered *weak* when the number of the lamella is not large enough to resist the gas flow [56,57].

In order to interpret these observations we need to recall that foams are thermodynamically meta-stable. They evolve irreversibly over time because the interfacial area in the lamella diminishes in order to minimize interfacial free energy [58]. The longevity of foam in porous media essentially relies on the stability of single foam films or lamellae. The stability of foam films depends on quantities and processes like surfactant concentration, salt concentration, adsorption kinetics, gravitational drainage, gas diffusion through foam films, surface forces (or capillary pressure) and fluctuations [59,60]. Before we assert the dominant factor responsible for the difference between CO_2 and N_2 foams it is worth reviewing how individual mechanisms could affect foam stability.

Coalescence and drainage: These two processes are responsible for the changes in degree of dispersion of gas bubbles in foam as they cause: (i) the diffusion of gas through the lamellae and (ii) collapse of liquid lamellae and subsequent coalescence of contiguous gas bubbles [61]. Pressure difference between bubbles of unequal size induces gas-transfer from small to larger bubbles. Even in the ideal situation of an initially perfectly ordered foam, comprised of uniform bubbles with a uniform gas pressure, finite size perturbation in bubble shape (e.g. due to irregularities and heterogeneity in porous media) would lead to an irreversible growth of the larger bubbles at the expense of the smaller [56]. This foam coarsening, the Oswald ripening, is unavoidable [37].

The mass-transfer rate of gas through foam films can be characterized by the film permeability *k*. Following to Princen and Mason [62] gas permeability depends on physical coefficients according to equation

$$k = \frac{k_H D}{h_w + 2D/k_{ml}} \tag{3}$$

where, D is the diffusion coefficient of the gas in the liquid phase, k_H is the Henry's coefficient, k_{ml} is the permeability of the surfactant monolayer to gas and h_w is the thickness of the liquid film. Eq. (3) shows that the permeation rate for thick foam films, ($2D/k_{ml} << h_w$), is mainly controlled by the liquid layer via D and k_H ($k \approx k_H D$), while for thin foam films ($2D/k_{ml} >> h_w$) the permeability of the monolayer ($k = k_H k_{ml}/2$) is the limiting factor.

The gas permeability of the foam films essentially depends on the solubility of the gas in the aqueous phase and the monolayer permeability. To compare the solubilities of the gases we may use the ratio of their their Henry's constants, $k_{H,CO_2}/k_{H,N_2} = 3.4\times10^{-2}/6.1\times10^{-4} = 55$. This implies that CO_2 is about *55* times more soluble in water than N_2 [46]. In the only published data, the transfer rate of CO_2 through the foam films stabilized by hexadecyltrimethylammonium bromide (HDTAB) in the presence of NaBr was measured to be about 60 times larger than that of N_2 [62,67].

The rather good agreement between the two ratios (solubility and film permeability ratio) suggests that coalescence rate of CO_2 foam bubbles must be much higher than than that of N_2 foam bubbles. Therefore this could be why CO_2 foam is weaker than N_2 foam. This is analogous to the situation whereof steam foam where water vapor can pass through lamellae by condensing on one side and evaporating on the other side [68]. A small amount of nitrogen is added to reduce this effect in steam foam [69] and in the beer industry [37,70]. The higher solubility of CO_2 could also explain why in CO_2 foam more pore volumes of gas are needed before the gas becomes visible in the core and also why the speed of the foam front is lower for CO_2 than for N_2. Indeed a considerable fraction of CO_2 dissolved in the surfactant solution before can be foamed since the amount of available gas for foaming is reduced.

In porous media the Plateau borders are connected throughout the pore space and form a conductive network. In response to the local pressure gradient and gravity the liquid starts to flow. Liquid depletion in turn increases the capillary suction pressure on the lamella, which may result in film rupture. Coarsening also has a strong influence on foam drainage for gases of large solubilities (e.g. CO_2) and small bubble sizes (*diameters <1 mm*) [63-65]. This coupling effect can shorten the lifetime of (CO_2)- foam.

The lamellae remain in the pore throats of porous media and ideally at equilibrium they will have no curvature and thus sustain no pressure drop. Therefore in the absence of the driving force the diffusion process stops. This may cause the foam remain *indefinitely* in the porous medium in the *absence of external disturbances* (in porous media heterogeneity and temperature fluctuations can be counted as external disturbances) [71,72].

Figure 10 shows a plot of the pressure drop over the entire core as a function of the average gas saturation in the core for low pressure CO_2 and N_2 foams respectively. Initially both foams show similar behavior, i.e., while the gas displaces the liquid the pressure drop remains low (weak foam). However, as time passes for similar gas fractions (above S_g*=0.30*), N_2 foam exhibits higher pressure drop over the core. This implies that 1) while a transition from weak foam to strong foam occurs in N_2 foam, CO_2 foam always remains weak and 2) CO_2 foam is coarser than N_2 foam in porous media due to more intense rupture of the foam films (lamellae), as discussed previously. Figure 11 provides a similar plot for high pressure experiments. Again in this case there is a gas saturation in which the transition from weak foam to strong foam occurs in N_2 foam (S_g*~0.35*). This saturation is higher than that of the low pressure N_2 foam presumably due to the differences in the flowrates. Seemingly, CO_2 continues to flow as a weak foam (or more accurately foamulsion) in the core.

Role of Interfacial tension: The interfacial tensions of the CO_2-water and the N_2-water systems exhibit different behavior. The interfacial tension of the N_2-water binary system does not vary considerably with pressure such that it can be assumed constant in the range of our experimental pressures [73,74]. Nevertheless, the interfacial tension between CO_2 and water depends strongly on pressure for pressures smaller than *10 MPa*, decreasing as the pressure increases (from 72 to about 20 mN/m), and displays an asymptotic behavior towards a constant value for higher pressures [75-77]. Even at low pressure of *1 bar* the presence of CO_2 above a surfactant solution may lower the interfacial tension possibly due to the surface hydrolysis of the surfactant [78]. The resistance to flow of the individual lamella in porous media is proportional to the surface tension [79]. It is interesting to mention that decrease in the interfacial tension leads to higher permeation of the gas molecules through the foam films and therefore may decrease the stability of foam [80]. Moreover, it has been observed that the relative permeability of CO_2 increases as the interfacial tension of the CO_2-water system decreases [77].

Wettability Alteration Effects: Part of the observed differences in CO_2 and N_2 foam experiments may be attributed to both, differences in the interfacial tension and differences in the wetting angles of the two gases, i.e., the value of $\sigma\cos\theta$, where σ is the gas-water interfacial tension and θ is the contact angle. Hildenbrand et al. [81] stated that for the N_2-water system the product of $\sigma\cos\theta$ exceeds the corresponding product for the CO_2-water system by a factor of *1.3-2.0*. This suggests that wettability of the clay part of the rock may change with injecting CO_2. Foam is more stable in water-wet rock than in intermediate (or oil) wet porous media [82-84]. If the medium is not water-wet the walls may cause the lamellae to detach and collapse [1]. Our experiments are done in Bentheimer sandstone that contains *1-4 wt%* of clay [85]. Therefore, injection of CO_2 affects the wettability of the cores. When the lamella moves across a non-wetting spot of the pores it ruptures by the pinch-off mechanism [35] lowering the resistance of foam to flow. It is important to remark that wettability and interfacial tension forces at the interface between liquid and rock may also affect bubble formation is also affected by [86]. Hence, it is possible that the rate of foam generation in CO_2 foam is different than N_2 foam due to wettability effects.

pH effects: Another factor that may affect the foam stability is the pH of the aqueous phase. When CO_2 is injected into a reservoir, CO_2 reacts with water and forms carbonic acid. This reaction may lower the pH of the brine down to 4.0 [87]. The value of pH may influence the foam film stability by affecting the disjoining pressure through screening of the van der Waals and electrostatic forces [60]. The pH changes could also influence the surfactant performance in porous media [88]. However, based on the experimental results it has been asserted in the literature that pH has little effect on foam viscosity [87], foam resistivity [89] or in general foam stability when the surfactant concentration is above the CMC [90].

Alteration of van der Waals forces: The disjoining pressure is a measure of stability of a foam film and strongly depends on the film thickness [58,61]. According to the DLVO theory this pressure has two components: repulsive electrostatic and attractive van der Waals forces [61]. The effect of gas type on the van der Waals component of the disjoining pressure can be evaluated using Hamaker's constant, which depends on the optical and dielectric properties of the aqueous and non-aqueous phases [91]. Since these properties for CO_2 and N_2 are different it has been hypothesized that the differences in the magnitude of the attractive van der Waals forces of the lamellae in CO_2 and N_2 foams cause the differences observed in the experiments [60]. The calculations of ref. [60] shows that the magnitude of screening of electrostatic forces for CO_2 is two times that of N_2, while screened Hamaker's constants indicate that van der Waals forces are six time lower for CO_2.

Type of surfactant: Different gases may show different foaming behavior with different surfactants. Although AOS surfactants have been previously used in CO_2 foam projects, it is possible that type of surfactant is responsible for the differences observed in the experiments.

Temperature effects: Temperature is another parameter that controls the foam stability by influencing the diffusion rate and adsorption of the surfactant molecules at the gas-water interface and rock surface. CO_2 dissolution in water is exothermic. The solution heat of CO_2 is given by

$$-\left(d\ln k_H / d(1/T)\right)_{CO_2} = \Delta H_{CO_2} / R = 2400K \rightarrow \Delta H_{CO_2} \approx 2.0\times10^4 J/mol$$

This implies that CO_2 dissolution can cause temperature increase of

$$\Delta T_{CO_2} = \frac{\Delta H_{CO_2}}{k_H c_{p,w}} = \frac{2\times10^4}{3400\times4.2\times10^6} \approx 0.15K/bar$$

A similar calculation for N_2 reads: $\Delta T_{N_2} \approx 0.00015K/bar$. Therefore, the temperature rise in the water due to CO_2 dissolution is more significant, especially at higher pressures. The increase in temperature can reduce the foam stability in porous media because (i) it can initiate the inter-bubble diffusion process by causing infinitesimal perturbation and thus disturbing the equilibrium and (ii) it increases the mass transfer rate through the bubbles. However, it should be noted that the temperature effects cannot completely be responsible for the differences in foaming behavior of CO_2 and N_2 since at low pressure the temperature effect will not be significant.

5. CONCLUSIONS

The foaming behavior of CO_2 and N_2 were comparatively studied in a sandstone core by the means of a CT scanner (X-ray). Alpha Olefin Sulfonate (AOS) was used as surfactant. It has been shown that injection of a slug of surfactant prior to CO_2 injection can reduce the CO_2 mobility, below and above its critical point. The two investigated gases exhibit different behavior in the porous medium. Foaming of CO_2 builds up lower pressure drop over the core at both low and high pressures when compared to N_2. Both gases require space to develop into foam. The space is longer for N_2 (large entrance effect) and increases

with increasing gas velocity. The CT images and calculated water saturation profiles reveal that N_2 foam displaces the liquid in a front-like manner (sharp-vertical interface) while the propagation front for CO_2 foam is not the exact front-like displacement at low pressure. Moreover, the ultimate production of N_2 foam is always higher than CO_2 foam. The observed differences in the foaming behavior of the two gases can be related to the differences in their nature, mainly solubility in water, interfacial tensions, pH effects, type of surfactant and the possible wettability effects. From these various factor solubility is most likely the most critical one because 1) part of the gas is dissolved in the aqueous phase and therefore when volumetric flowrates of two gases are the same the local gas velocities will be different, i.e., the amount of available CO_2 for foaming will be lower than N_2 at similar PVs and 2) it significantly affects the gas permeability coefficient and thus the foam stability.

6. ACKNOWLEDGMENT

This research was carried out as part of a project funded by Delft Earth Research and Shell International Exploration and Production, Rijswijk. We thank the technicians of the Dietz laboratory of our faculty for their support.

7. REFERENCES

1. W.R. Rossen, Foams in Enhanced Oil Recovery, In: Foams: Theory Measurement and Applications, R.K. Prud'homme and S. Khan (Eds), Marcel Dekker, New York City (1996).
2. A.R. Kovscek and C.J. Radke, Fundamentals of foam transport in porous media, In: Foams: Fundamentals and applications in the Petroleum Industry, ACS Advances in Chemistry Series, N.242, American Society (1994).
3. Falls, G.J. Hirasaki, T.W. Patzek, D.A. Gauglitz, D.D. Miller, J. Ratulowski, SPE Res. Eng., 176-190 (1985).
4. C.L. Smith, J.L. Anderson, and P.G. Roberts, SPE 2751, Presented at the 1969 SPE California Regional Meeting, San Francisco, 6–7 November.
5. S.L. Wellington and H.J. Vinegar, Surfactant-Induced Mobility Control for Carbon Dioxide Studied with Computerized Tomography. In Surfactant Based Mobility Control – Progress in Miscible Flood Enhanced Oil Recovery; Smith, D.H., Eds.; ACS Symposium Series 373; American Chemical Society: Washington, 1988; pp.344-35.
6. M.G. Bernadiner, K.E. Thompson, and H.S. Fogler, SPE Prod. Eng. 350–356, November 1992.
7. R. Gdanski, Oil Gas J. 85–89, 6 September 1993.
8. W.R. Rossen and W.W. Wang, SPE J, 4(2), June 1999.
9. T.W. Patzek and N.A. Myhill, SPE 18786, Presented at the SPE California Regional Meeting held In Bakersfield, California, April 5-7, 1989.
10. R. Liu, H. Liu, X. Li, Z. Fan, SPE 114800, Presented at the SPE Asia Pacific Oil & Gas Conference and Exhibition held in Pert, Australia, 2008.
11. F.D. Martin, J.E. Stevens, and K.J. Harpole, SPE Reservoir Engineering, Nov. 1995.
12. R.W. Klusman, Energy Conversion and Management, 44, 1921–1940 (2003).
13. M.H. Holtz, P.K. Nance, R.J. Finley, Environ Geosci, 8 (3), 187-199 (2001).
14. H. Koide H and K. Yamazaki, Environ Geosci, 8 (3), 218-224 (2001).
15. K. Preuss and J. Garcia, Environ. Geology, 42, 282-295 (2002).
16. J.M. Nordbotten, M.A. Celia, S.B. Bachu, H. Dahle, Environ. Sci. Technol., 39 (2), 602-611 (2005).
17. W.R. Rossen and P.A. Gauglitz, AIChE, 36, 1176-88 (1990).
18. S.I. Chou, SPE 22628, SPE Annual Technical Conference and Exhibition, Dallas, Oct. 6-9 (1991).
19. A.T. Turta and A.K. Singhal, SPE 48895, SPE International Conference and Exhibition, China, Beijing, 2-6 Nov. 1998.
20. Svortol, F. Vassenden, K. Mannhardt, SPE 35400 , SPE/DOE tenth symposium on improved oil recovery : Tulsa OK, 21-24 April 1996
21. Blaker, H.K. Celius, T. Liet, H.A. Martinsen, L. Ramsussen, F. Vassenden, SPE 56478 (SPE 78824), SPE annual technical conference and exhibition : Houston TX, 3-6 October 1999.

22. M.G. Aarra, A. Skauge, H.A. Martinsen, SPE 77695, SPE Annual Technical Conference and Exhibition, San Antonio, Texas , 29 September-2 October 2002,
23. C.S. Matthews, In: Enhanced Oil Recovery II, Processes and Operations, E.C. Donaldson, G.V. Chilingarian, T.F. Yen, Elsevier Science Publ. Co., New York (1989).
24. J.P. Heller, CO2 Foams in Enhanced Oil Recovery, In: Foams: Fundamentals and Applications in the Petroleum Industry, L.L. Schramm (ed), ACS Advances in Chemistry Series, 3, No. 242, Am. Chemical Soc., Washington, D.C. (1994). D.G.
25. Huh and L.L. Handy, SPE Reservoir Engineering, February 1989.
26. P.Q. Nguyen, Dynamics of foam in porous media, PhD Dissertation, Delft University of Tech., The Netherlands, 2004.
27. D.X. Du, A. Naderi Beni, R. Farajzadeh, P.L.J. Zitha, Ind. Eng. Chem. Res., 47, 6298-6306 (2008)
28. P.Q. Nguyen, P.K. Currie, M. Buijse, P.L.J. Zitha, J. Petrol. Sci. Eng., 58, 119-132 (2007).
29. T. Myers and C.J. Radke, Ind. Eng. Chem. Res., 39 (8), 2725 -2741 (2000)
30. S. Tortopidis and D.C. Shallcross, SPE 28811, Asia Pacific Oil and Gas Conference, Australia, 7-10 November 1994.
31. O. Fergui, H. Bertin, M. Quintard, J. Petrol. Sci. Eng., 20, 9-29 (1998).
32. C.A. Irani and C. Solomon, SPE/DOE 14962, 5th Symposium on EOR, Tulsa, OK, 20-23 April 1986.
33. S.H. Raza, In. Soc. Pet. Eng., vol 10, no. 4, December 1970.
34. G.C. Wang, SPE 12645, 4th Symposium on EOR, Tulsa, OK, 15-18 April 1986.
35. T. Myers, The role of residual oil in the mechanistic simulation of foam flow in porous media: Experiment and simulation with the population balance method, PhD Dissertation, University of California, Berkeley, USA, 1999.
36. R. Krastev, Private Communication (2008).
37. D. Weaire and S. Hutzler, The Physics of Foams, Oxford University Press (1999).
38. Saint-Jamles and D. Langevin, Condens. Matter Phys., 14, 9397-9412 (2002).
39. M.I. Kuhlan, A.H. Falls, S.K. Hara, T.G. Monger, J.K. Borchardt, SPE/DOE 20192, Presented at the SPE/DOE Symposium on Enhanced Oil Recovery, Tulsa, OK, April 22-25 (1990).
40. L.W. Holm and W.H. Garrison, SPE Reservoir Engineering, 3, 112 (1988).
41. P.A. Gauglitz, F. Friedmann, S.I. Kam, W.R. Rossen, SPE 75177, SPE/DOE Improved Oil Recovery Symposium, Tulsa, Oklahoma, U.S. April 13-17, 2002.
42. Hutchins, R.D.; Miller, M.J. A Circulating Foam Loop for Evaluating Foam at Conditions of Use. SPE Production & Facilities, 20, 286 (2005).
43. Prieditis and G.S. Paulett, SPE 24178, SPE/DOE Eighth Symposium on Enhanced Oil Recovery, Tulsa, OK, 1992.
44. R. Farajzadeh, R. Krastev, P.L.J. Zitha, Colloids Surf. A, 324, 35-40 (2008).
45. D.X. Du, Private Communication (2007).
46. R. Sander, Compilation of Henry's Law Constants for Inorganic and Organic Species of Potential Importance in Environmental Chemistry, http://www.mpch-mainz.mpg.de/%7Esander/res/henry.html, Version 3, 1999, p57 (last date accessed September 2008)
47. R.A. Brooks, G.H. Weiss, A.J. Talbert, J. Comput. Assist. Tomog., 2, 577 (1978).
48. P.L.J. Zitha, Q.P. Nguyen, P.K. Currie, M.A. Buijse, Transport in Porous Media, 64, 301-313 (2006).
49. O. G. Apaydin and A. R. Kovscek, Transport in Porous Media, 43: 511–536 (2001).
50. J.J. Douglas and R.J. Wagner, Petrol. Transact., AIME, 213, 96–102 (1958).
51. F.M.J. Perkins, Petrol. Trans., AIME, 210, 409–411 (1957).
52. M. Mahmoodi Nick, Immiscible Foam for EOR, MSc thesis, Delft University of Technology, The Netherlands, July 200

53. B.E. Poling, J.M. Prausnitz, J.P. O'Connell, The properties of gases and liquids, 5th Ed., McGraw Hills, (2000).
54. R. Span and W. Wagner, J. Phys. Chem. Ref. Data, 25 (6), 1509-1596 (1996).
55. N. Spycher, K. Pruess, J. Ennis-King, Geochimica et Cosmochimica Acta, 67 (16), 3015-3031 (2003).
56. J.P. Heller and M.S. Kuntamukkula, Ind. Eng. Chem. Res., 26, 318-25 (1987).
57. K.R. Kibodeaux, Experimental and theoretical studies of foam mechanisms in enhanced oil recovery and matrix acidization application, PhD Dissertation, University of Texas at Austin, The US, 1997.
58. K.G. Kornev, A.V. Niemark, A.N. Rozhkov, Adv. Colloid Interf. Sci., 82, 127-187 (1999).
59. R.v. Klitzing and H.-J. Müller, Curr. Opin. Colloid In., 7, 42-9 (2002).
60. A.S. Aronson, V. Bergeron, M.E. Fagan, C.J. Radke, Colloids Surf. A, 83, 109-20 (1994).
61. A.J. de Vries, in: Foam stability, a fundamental investigation of the factors controling the stability of foams, Delft (The Netherlands), Communication No. 326 (1957).
62. H. M. Princen and S. G. Mason, J. Colloid Sci, 20 (1965) 353.
63. S. Higenfeldt, S.A. Koehler, H.A. Stone, Phys. Rev. Lett., 86 (20), 4704-7 (2001).
64. F.G. Gandolfo and H.L. Rosano, J. Colloid Interf. Sci., 194, 31-36 (1997).
65. M.U. Vera and D.J. Durian, Phys. Rev. Lett., 88 (8), 088304-1-4 (2002).
66. G. Maurdev, A.Saint-Jalmes, D. Langevin, J. Colloid Interf. Sci., 300, 735-743 (2006).
67. H. M. Princen, J. Th. G. Overbeek and S. G. Mason, J. Colloid Int. Sci, 24, 125-130 (1967).
68. G.J. Hirasaki, Private Communication (2008).
69. A.H. Falls, J.B. Lawson, H.J. Hirasaki, J. Pet. Tech., 95-104 (1988).
70. Teng and J.H. Dokos, US Patent no. 4610888, 1986.
71. D. Cohen, T.W. Patzek, C.J. Radke, J. Colloid Interf. Sci., 179, 357-373 (1996).
72. D. Cohen, T.W. Patzek, C.J. Radke, Transport in Porous Media, 28, 253-284 (1997).
73. R. Masoudi and A. King, J. Phys. Chem., 78, 2262-6 (1974).
74. W.L. Masterton, J. Bianchi, E.J. Slowinski, J. Phys. Chem., 67, 615-8 (1963).
75. S.R.P. da Rocha, K.L. Harrison, K.P. Johnston, Langmuir, 15, 2 (1999).
76. P. Chiquet, J-L. Daridon, D. Broseta, S. Thibeau, Energy Conversion and Management, 48, 736–744 (2007).
77. S. Bachu and B. Bennion, Environ Geol, 54, 1707–1722 (2008).
78. T. Gilanyi, Chr. Stergiopoulos, E. Wolfram, Colloid and Polymer Sci, 254, 1018-1023 (1976)
79. G.J. Hirasaki and J.B. Lawson, SPE J, 176-190 (1985).
80. R. Krustev, D. Platikanov and M. Nedyalkov, Colloids Surf. A, 383 123-124 (1997).
81. Hildenbrand, S. Schlomer, B.M. Kroos, R. Littke, Geofluids, 4, 46161-80 (2004).
82. F.E. Suffridge, K.T. Raterman, G.C. Russell, SPE 19691 (1989).
83. Manhardt and J.J. Novosad, In Situ, 18(2), 145-183 (1994).
84. L.L. Schramm and K. Mannhardt, J. Petrol. Sci and Eng., 15, 101-113 (1996).
85. G. Al-Muntasheri, Polymer gels for water control: NMR and CT scan studies, PhD dissertation, Delft University of Technology, The Netherlands (2008).
86. H. Kogawa, T. Shobu, M. Futakawa, A. Bucheeri, K. Haga, Takashi Naoe, J. Nuclear Materials, 377, 189-194 (2008).
87. C.N. Fredd, M.J. Miller, B.W. Quintero, SPE 86493, SPE International Symposium and Exhibition on Formation Damage Control, Lafayette, Louisiana, U.S. February 18-20, 2004.
88. C.J. Radke, Private Communication (2008).

89. T. Zhu, A. Strycker, C.J. Raible, K. Vineyard, SPE 39680, SPE/DOE Improved Oil Recovery Symposium, Tulsa, OK, U.S. April 19-22, 199

90. Y. Liu and R.B. Grigg, SPE 93095, SPE International Symposium on Oilfield Chemistry, the Woodlands, Texas, U.S., February 2-4, 2005.

91. J. Israelachvili, Intermolecular and Surface Forces, Academic Press: London, 1991.

92. R. Farajzadeh, R. Krastev, P.L.J. Zitha, Adv. Colloid. Interf. Sci, 137, 27-44 (2008).